I J C T A, 9(34) 2016, pp. 105-117

Efficiency Enhancement of Wireless Charging System By Applying Phase-shift and Amplitude Control Using Fuzzy Logic

S. Sanjeeva Rayudu[1], M. Sai sandeep[2] and G. Bhargavi[3]

ABSTRACT

Wireless power transfer is the technology that enables a power source to transmit electromagnetic energy to an electrical load across an air gap without interconnecting cords.However, its widespread application is hampered due to the relatively low efficiency of current Wireless power transfer (WPT) systems this study presents a concept to maximize the efficiency as well as to increase the amount of extractable power of a WPT system operating in no resonant operationby applying phase shift and amplitude control. The proposed method is based on actively modifying the equivalent secondary side load impedance by controlling the phase-shift of the active rectifier and its output voltage level. Simulation results are shown for the proposed concept. A fuzzy controller is used and the results are compared to other controllers.

Key words: Dc-dc power converters, impedance matching, inductive power transmission, phase-shift control, reactive power control, rectifiers, wireless charging, and Fuzzy logic.

I. INTRODUCTION

Remote force exchange is the innovation that empowers a force supply to transmit attractive power vitality to an electrical burden over an air hole, while not interconnecting lines. This innovation is pulling in an extensive variety of utilizations, from low-control toothbrush to high-control electrical vehicles because of its comfort and better client experience. Various parts of these frameworks are characterized by numerous principles that are either taking into account non-full or inductive force exchange (IPT), like the qi standard or on resounding force exchange (RPT), like the Rezencestandar. These days, remote charging is quickly advancing from hypotheses toward standard components on mechanical items, particularly cellular telephones and versatile sensible gadgets. In 2014, a few driving advanced cell creators, as Samsung, Apple and Huawei, started to unleash new-era gadgets highlighted with inbuilt remote charging capacity. In order to affirm capacity of different transmitter and recipient gadgets, these guidelines layout parameters like the voltage fluctuate, the vital circuit structure, and along these lines the in operation recurrence of the framework.

In spite of the fact that WPT has been widely contemplated as of late, less consideration has been paid to the enhancement of a whole remote charging framework, beginning from a dc information supply to charging electric battery at the yield. In, a vitality agreeable remote charging framework has been introduced however exclusively mechanical accessible components are utilized and no propelled advancement procedures have been connected to expand the framework intensity and the extractable yield power.

In a remote charging framework the proficiency and the measure of force exchanged to the yield are impacted by the source (transmitter) and burden (recipient) impedances. In, the heap impedance is thought to be absolutely resistive and, in this manner, effectiveness changes are accounted for by just altering the

* Assistant Professor, Dept. EEE, A.I.T.S-Rajampet, A.P, INDIA.

** PG Student, Dept. EEE, A.I.T.S-Rajampet, A.P, INDIA.

resistive part of the heap impedance. Be that as it may, this methodology does not yield ideal proficiency for the entire working extent, since just the resistive part of the heap impedance is adjusted and the receptive part is not considered by any stretch of the imagination. The most extreme measure of force can be exchanged by changing the heap impedance to coordinate the mind boggling conjugate of the source impedance.

An impedance change unit is connected into scratch off the responsive part of the impedance and from that point to adjust the resistive part with a specific end goal to yield most extreme force exchange. Extra changes to the productivity of a WPT framework are acquired by effectively altering the responsive part of the heap impedance. Here we are utilizing the fuzzy controller contrasted with different controllers.

A stage shift control approach, rather than a routine controlling technique, is connected to the dynamic rectifier on the auxiliary part of a RPT framework. This framework is utilized to accomplish proficiency improvements by altering the optional side reverberation recurrence, however then again it furthermore affects the proportional burden impedance. Since the stage movement is that the main control parameter, the resistive likewise on the grounds that the receptive a part of the proportional burden electric resistance region unit in the meantime changed.

Consequently, these 2 parameters can't be controlled on an individual premise furthermore the reason for most power isn't came to for the most part. The exhibited approachaccept non-resounding operation (IPT) and depends on the vitality standard details. When connected to a RPT framework agent precisely at reverberation recurrence, the receptive a part of the framework is intrinsically salaried, and thus the proposed approach indicates indistinguishable conduct as a synchronous rectifier. An enhanced administration technique to effectively manage the resistive comparably on the grounds that the receptive a part of the equal burden impedance is acquainted so as with upgrade the framework execution.

II. THEORETICAL ANALYSIS

In this part the modeling of WPT system is introduced and the theoretical conditions for calculating the maximum efficiency and the maximum power transfer are provided. A block diagram of the examined system is shown in Fig. 1.

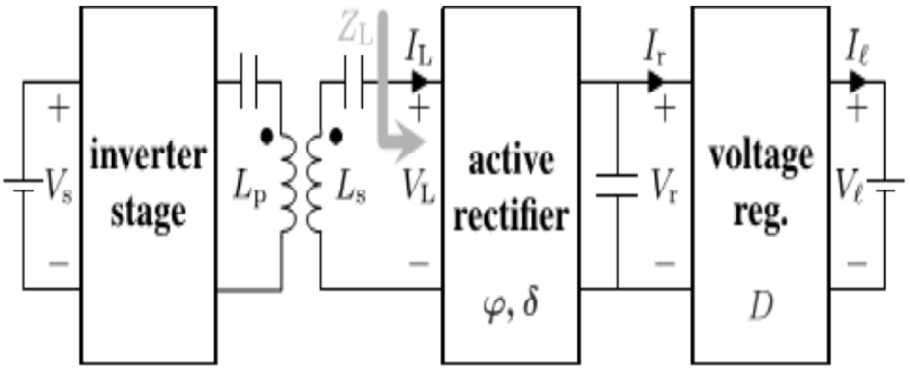

Figure 1: Schematic block diagram of the overall WPT system including an inverter stage driving the primary side resonance circuit, an active rectifier and a dc–dc converter at the secondary side

A. System Modeling

The first harmonic approximation is used to the WPT system shown in Fig. 1. This method solely considers the fundamental element of the input voltage and replaces the active rectifier as well as the dc–dc converter by an equivalent harmonic electric resistance $ZL=R_L+jX_L$. The applied simplification is sufficiently correct for high quality issue resonant circuits that operate close to resonance frequency. This study focuses on the

steady-state analysis of a series-series resonant WPT system as shown in Fig. 2; however the planned concept is applicable to each topology.

The curved voltage supply V_{in} is an equivalent root mean sq. (RMS) input voltage that is driving the first side resonance circuit. The series resistances R_p and Rs represent the overall parasitic resistances of the first and therefore the secondary facet resonance circuit. The series capacitors Cp and cesium square measure needed to tune the resonance frequency of the first and therefore the secondary facet, whereas the mutual inductance M depends on the coupling issue k=ML$_p$Ls, that is influenced by the geometry, the distance, and therefore the alignment of the inductors disc and Ls.

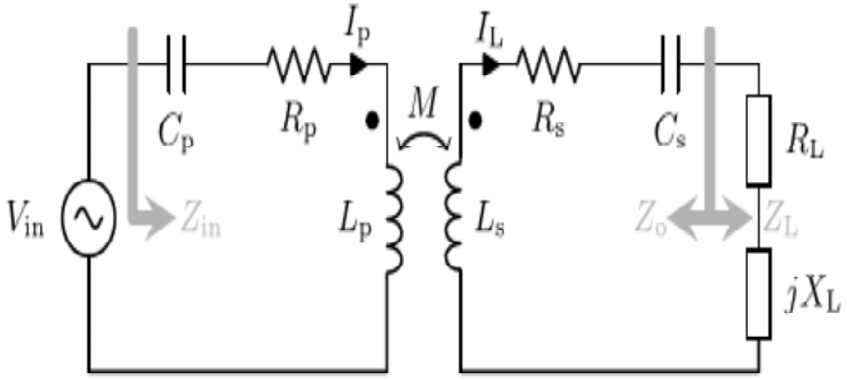

Figure 2: Equivalent circuit model of a series-series tuned WPT system based on the first harmonic approximation

The open-circuit impedances of the primary and secondary side resonance circuits are defined as

$$Z_p = R_p + jX_p = R_p + j\left(\omega L_p - \frac{1}{\omega C_p}\right) \quad (1)$$

$$Z_s = R_s + jX_s = R_s + j\left(\omega L_s - \frac{1}{\omega C_s}\right)(\quad (2)$$

The equivalent load impedance of the WPT system can be modeled as a complex impedance ZL=R_L+jX_L,. The impedances Z_{in} and Z_o, as shown in Fig. 2, are the equivalent impedances seen by the source and by the output, respectively.

$$Z_{in} = Z_P + \frac{X_m^2}{Z_S + Z_L} \quad (3)$$

$$Z_0 = Z_S + \frac{X_m^2}{Z_P} \quad (4)$$

Where X_m= ωM represents the mutual impedance of the coupled inductors. To further simplify the ac circuit model in Fig. 2, the coupled inductors L_p and L_s can be modeled as equivalent current controlled voltage sources at the primary and the secondary side as shown in Fig. 3.

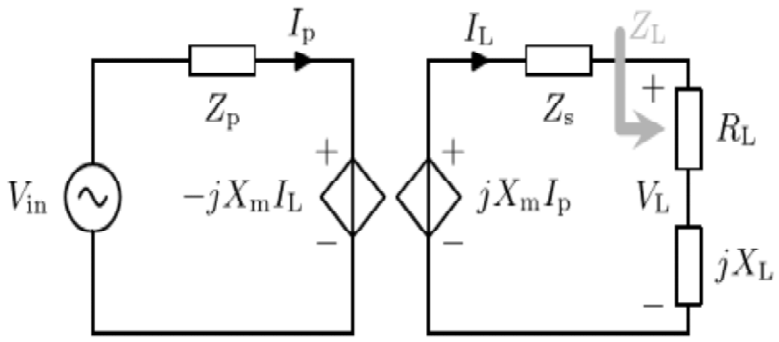

Figure 3: Circuit model of the WPT system using two equivalent sources to model the coupling between the inductors L_p and L_s

The induced voltage at the secondary side is influenced by the primary side current Ip and can be denoted by $jX_m I_p$.On the other hand, the current at the secondary side I_L also causes an induced voltage at the primary side inductor which is determined by $-jX_m I_L$.

B. Efficiency and Extractable Power

In order to analyze the system performance, the input and output power of the WPT system are derived as operate of the resistive part R_L and also the reactive part X_L of the equivalent load electrical phenomenon. The subsequentrelations for the mean input power Pin, respectively the mean output power Pout, are supported the equivalent model in Fig. 3 and are given as

$$P_{in}(R_L, X_L) = \frac{V_{in}^2[R_p + R_e\{Z_r\}]}{[R_p + R_e\{Z_r\}]^2 + [X_p + I_m\{Z_r\}]^2} \tag{5}$$

$$P_{out}(R_L, X_L) = \frac{V_{in}^2 X_m^2 R_L}{den} \tag{6}$$

And V_{in} denotes the RMS value of the input voltage of the system. The impedance Z_r represents the reflected impedance from the secondary to the primary side which can be derived as

$$Z_r = \frac{X_m^2}{Z_S + Z_L} \tag{7}$$

It is well known from the literature that the maximum output power can be achieved by a conjugate matching of the equivalent load and output impedance of the system ($Z_L = Z*o$). With the relations (5) and (6) for the input and output power, the system efficiency as a function of the load impedance can be expressed as

$$\eta(R_L, X_L) = \frac{X_m^2 R_L}{[(R_S + R_L)^2 + (X_S + X_L)^2] + X_m^2 (R_S + R_L)} \tag{8}$$

In case only the efficiency is considered, (8) can be maximized by canceling the reactive part ($X_L = -X_s$)and by solely optimizing the real part R_L of the equivalent load. The optimal load resistance can then be derived by setting the derivative of (8) to zero which yields

$$R_{L,opt} = \sqrt{R_s^2 + \frac{R_s}{R_p} X_m^2} \tag{9}$$

If the output power is varied by altering the load resistance R_L, the efficiency decreases and the system does not operate at the optimum efficiency for this particular value of the output power. It is worth noting that the conditions ($R_L = R_L$, opt, $X_L = -X_s$) for maximum efficiency, and ($Z_L = Z_o$) for maximum power transfer are in general not fulfilled at the same time.

III. PROPOSED CONCEPT

In this section synchronous rectification is in brief reviewed and, thereafter, the proposed concept for controlling the equivalent load impedance to optimize the efficiency and to increase the power transfer capability is mentioned very well. Simulation results are shown for a WPT system supported the k_i low-power specifications, operating at a frequency of 140 k_c with a resonance frequency of one hundred kc. The values used for simulation are based on the parameters of the experimental setup that are summarized in Table II in Section V.

A. Synchronous Rectification

Synchronous rectification is a commonly used technique to control an active rectifier, where the switches of the full bridge are driven according to the zero crossings of the rectifier input current I_L. Thus, the controller forces the current I_L and the voltage V_L at the input of the rectifier to be in phase ($\phi = 0$), which

results in a purely resistive behavior of the rectifier without compensation of the reactive part ($Z_L = R_L + j0$). Fig. 4 schematically illustrates the key waveforms of the synchronous rectification approach. To obtain the maximum efficiency for every point of the output power Pout the rectified voltage V_r is adjusted by controlling the duty cycle D of the dc–dc converter.

B. Proposed Concept

Recent research has shown the possibility to improve the performance of a WPT system by introducing a phase-shift between the primary and secondary side voltages. However, this method does not allow to separately controlling the resistive and reactive part of the equivalent load impedance, whereas in the proposed concept the overall impedance is controlled.

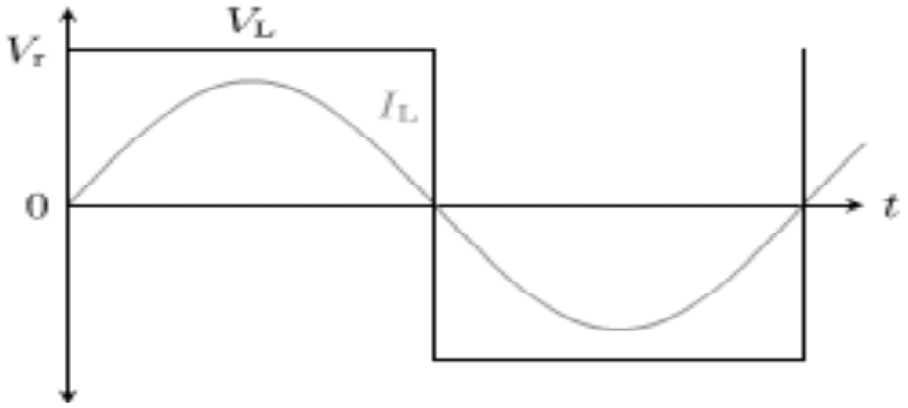

Figure 4: Rectifier input voltage V_L and current I_L for synchronous rectification ($\phi = 0$)

By defining the phase-shift ϕ as the angle between the first harmonic of the input current I_L and the voltage V_L of the active rectifier we derived an analytical expression for the equivalent input impedance of the active rectifier

$$Z_L(\varphi, V_r) = R_S + jX_L = \frac{V_L^{(1)}}{I_L^{(1)}} = \frac{4}{\pi}\frac{V_r}{I_L^{(1)}} e^{-j\varphi} = \frac{4}{\pi}\frac{V_r}{I_L^{(1)}}(\cos(\varphi) - j\sin(\varphi)) \tag{10}$$

Where $V_L^{(1)}$ and $I_L^{(1)}$ represent the amplitude of the first harmonic of the voltage V_L and the current I_L. By analyzing (10), it can be observed that a variation in the phase results in a change of the resistive as well as the reactive part of the equivalent load impedance. This behavior limits the optimization possibilities in case only the phase is actively controlled. On the other hand (10) shows the possibility to further improve the system by modifying a second parameter, the rectified voltage Vr.

By correctly adjusting D or δ the same value of rectified voltage Vr and hence the same equivalent resistance R_L can be achieved. The fundamental component of the rectifier input voltage V_L for the case of the duty cycle D control [see Fig. 5(a)] and the δ control [see Fig. 5(b)] can be denoted by

$$V_L^{(1)}(\varphi, D) = \frac{4}{\pi} V_r e^{-j\varphi} = \frac{4}{\pi}\frac{V_l}{D} e^{-j\varphi} \tag{11}$$

$$V_L^{(1)}(\varphi, \delta) = \frac{4}{\pi} V_r \sin(\delta/2)\, e^{-j\varphi} \tag{12}$$

Where $0 \le D \le 1$ and $0 \le \delta \le \pi$. Consequently, both of the presented control approaches can be used to regulate the rectified VoltageVr, but in this study the impact of the duty cycle D of the employed dc–dc converter is investigated in detail. The relation between the voltage regulator input (Vr) and output voltage

(V) affects the resistive part of the equivalent load impedance. Hence, a change in the rectified voltage can be used to modify the equivalent load resistance R_L.

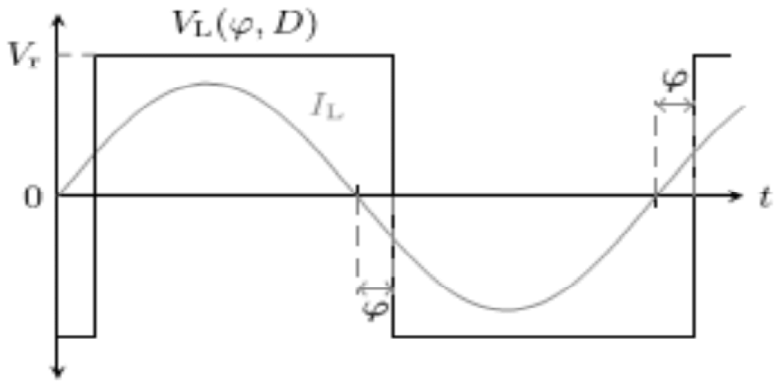

(a)

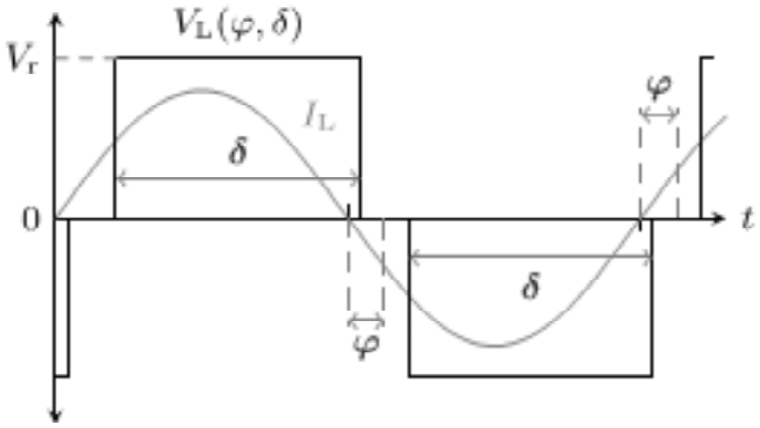

(b)

Figure 5: Schematic illustration of the key waveforms of the proposed method. (a) Voltage V_L and current I_L at the input of the rectifier utilizing the duty cycle D of the dc–dc converter to control the amplitude of the rectified voltage Vr. (b) Voltage V_L and current I_L at the input of the rectifier using the duty cycle δ of the active rectifier to adjust the rectified voltage Vr

IV. OPTIMIZATION STRATEGY

The first approach is based on the numerical optimization of the efficiency for a given output power using the resistive and reactive part of the equivalent load impedance. Since it is not straightforward to obtain the values of R_L and X_L during steady state, a second optimization method is introduced, where the rectifier input current IL is optimized as a function of the phase-shift ϕ and the rectified voltage Vr. These two measurable parameters can be used to achieve the maximum efficiency of the system for every value of the output power. It is worth noting that both presented optimization methods yield the same performance.

A. Optimization of the Resistive and Reactive Part

By controlling the resistive as well as the reactive part of the equivalent load impedance it is possible to optimize the system efficiency for a desired value of the output power. In order to calculate the optimum load impedance a constrained optimization process for every desired value of the output power is used.

Mathematically, this constrained optimization can be formulated as

$$Z_{L,opt}(P_{out}) = \underset{R_L, X_L}{\arg\max}\, (\eta(R_L, X_L)|P_{out}) \tag{13}$$

Fig. 6 presents the results of the constrained optimization process in (13) at a constant operating frequency of 140 kHz for a relatively high coupling factor k = 0.6 and a low coupling factor of k = 0.3

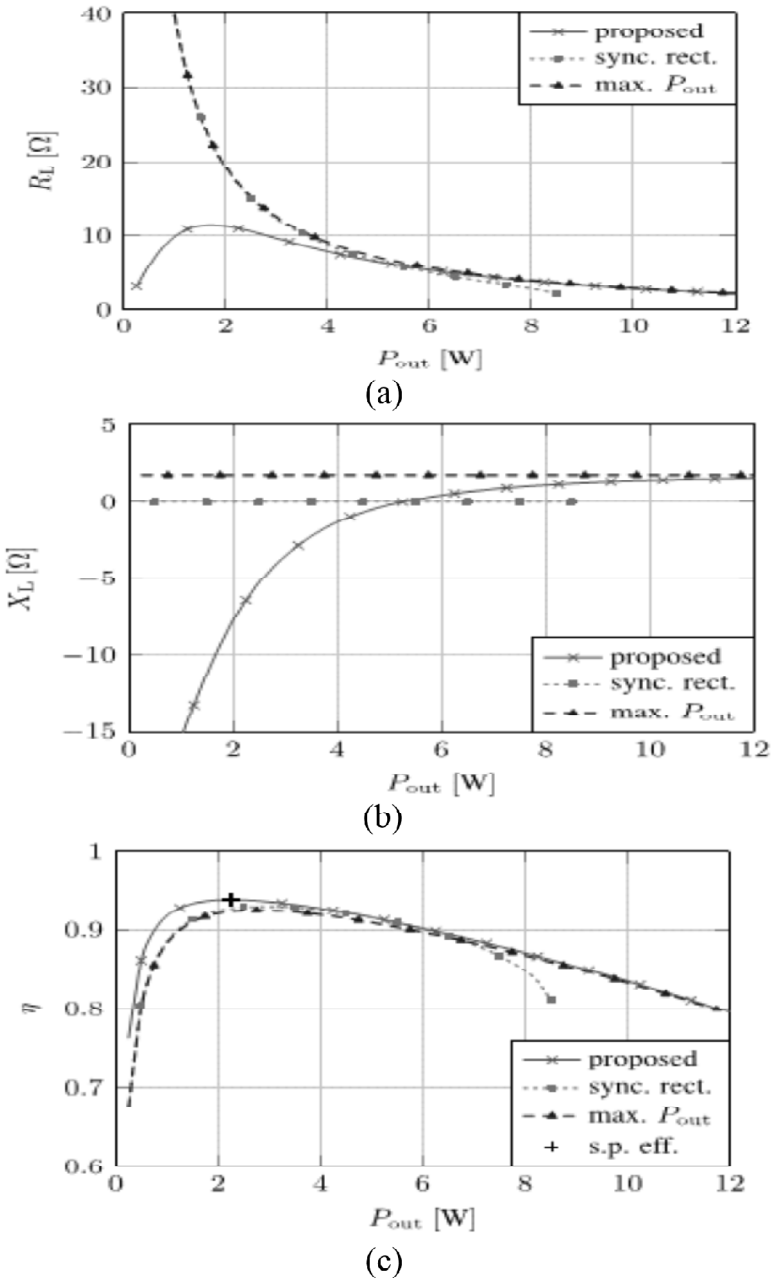

Figure 6: Impedance behavior and efficiency of the proposed concept compared to the maximum power approach and a synchronous rectifier. (a) Resistive part R_L over output power Pout for k = 0.6. (b) Reactive part X_L over output power Pout for k = 0.6. (c) Efficiency η over output power Pout for k = 0.6

The plots compare the impedance behavior as well as the achieved efficiency of the maximum power approach (conjugate matching of load and output impedances $Z_L = Z_0^*$ and optimizing R_L), the synchronous rectification approach (purely resistive R_L) and the proposed approach (optimizing both, the resistive and the reactive part).

Additionally, the point of maximum efficiency, obtained with the single-point optimization approach ($R_L = R_{L,opt}$, $X_L = -Xs$), is marked in the plots. Fig. 6(a) and (b) illustrates the behavior of the resistive and the reactive part, respectively, over the output power for a tightly coupled system (k = 0.6). The efficiency

of the different approaches in dependence on the output power is shown in Fig. 6(c). Fig. 6(d)–(f) presents the results for the same system with a lower coupling factor k = 0.3. The variation of the phase-shift adds an additional degree of freedom for the proposed control method, thus achieving an increased overall efficiency and a higher power transfer capability when compared to the conventional optimization approaches. For tight coupling (k = 0.6), the synchronous rectification achieves a lower system efficiency in the low power region as well as at the end of the medium power range when compared to the proposed method.

B. Optimization of the Phase-Shift and Rectified Voltage

This section introduces a second possibility to solve the constrained optimization problem in (13) based on measurable system parameters. In this approach, the optimal rectifier input current $I_{L,opt}$ and the optimal load impedance $Z_{L,opt}$ in dependence on the phase-shift ϕ and the rectified voltage Vr are derived to obtain the highest possible system efficiency for every value of the desired output power. To obtain the optimal system parameters, the system in Fig. 2 is represented as a two-port network which can be denoted in matrix form as

$$\begin{pmatrix} I_p \\ V_L \end{pmatrix} = \begin{pmatrix} Y_{11} & A_{12} \\ A_{21} & -Z_{22} \end{pmatrix} \begin{pmatrix} V_{in} \\ I_L \end{pmatrix} \tag{14}$$

Where the gain $A_{12} = A_{21}$ represents the ratio of the input current Ip to the output current I_L if the primary side is shorted, respectively the ratio of the secondary side voltage V_L to the primary side voltage V_{in} in case the secondary side is open. A_{12} can be calculated by

$$A_{12} = \frac{jX_m}{R_p + j(X_p + X_m)} \tag{15}$$

The impedance Z_{22} represents the output impedance of the wireless link in case the primary side is shorted, it can be derived as

$$Z_{22} = \frac{jX_m Z_p}{R_p + j(X_p + X_m)} \tag{16}$$

In order to calculate the optimum value of the impedance for every value of the output power an analytic solution for the constrained optimization process in (13) has been derived based on Lagrangian optimization methods. Since the efficiency is defined as the ratio between the input and output power, and Pout is a fixed value during the optimization process, the efficiency can be maximized by minimizing the input power Pin. Hence, the objective and the constraint for the Lagrangian optimization can be denoted by

$$P_{in} = R_e\{V_{in}^* I_P\} = V_{in} R_e\{I_p\} \tag{17}$$

$$P_{out} = R_e\{V_L^* I_L\} = constant \tag{18}$$

Where the phase of the input voltage V_{in} is referenced as 0° during the calculations, and hence V_{in} is purely real. For the proposed system a constant input voltage Vin, a constant coupling factor k and a constant operating frequency are assumed and hence the input power in (17) can be optimized by minimizing the primary side current Ip .

After solving the constrained optimization problem in (17) and (18), the optimized output current IL,opt(Pout,Vin)=ILR,opt(Pout,Vin)+jILI,opt(Pout,Vi) for a given amount of output power and a constant input voltage can be calculated as

$$I_{L,opt}^R(P_{out}, V_{in}) = V_{in} \frac{R_e\{A_{12}\}\left[-\sqrt{1-\frac{4P_{out}R_e\{Z_{22}\}}{V_{in}^2|A_{12}|^2}}+1\right]}{2R_e\{Z_{22}\}} \tag{19}$$

$$I_{L,opt}^I(P_{out}, V_{in}) = V_{in} \frac{I_m\{A_{12}\}\left[1+\sqrt{1-\frac{4P_{out}R_e\{Z_{22}\}}{V_{in}^2|A_{12}|^2}}+1\right]}{2R_e\{Z_{22}\}} \tag{20}$$

Where *I*R L,opt denotes the real and *I*LI ,opt the imaginary part of the current *I*L,opt . With (19) and (20) the optimum equivalent load impedance to achieve the maximum efficiency for a given amount of output power can be derived as

$$Z_L opt(P_{out} V_{in}) = \frac{A_{12} V_{in}}{I_{L,opt}(P_{out} V_{in})} - Z_{22} \quad (21)$$

The values of the rectified voltage Vr and the duty cycle D of the dc–dc converter are measurable on the prototyping system during steady-state operation. Hence, the point of maximum efficiency for every value of output power can be obtained on hardware and compared to the theoretical results.

V. FUZZY LOGIC CONTROLLER

In FLC, basic control action is determined by a set of linguistic rules. These rules are determined by the system. Since the numerical variables are converted into linguistic variables, mathematical modeling of the system is not required in FC. The FLC comprises of three parts: Fuzzification, interference engine and Defuzzificaion. The FC is characterized as i. seven fuzzy sets for each input and output. ii. Triangular membership functions for simplicity. iii. Fuzzification using continuous universe of discourse. iv. Implication using Mamdani's, 'min' operator. v. Defuzzificaion using the height method.

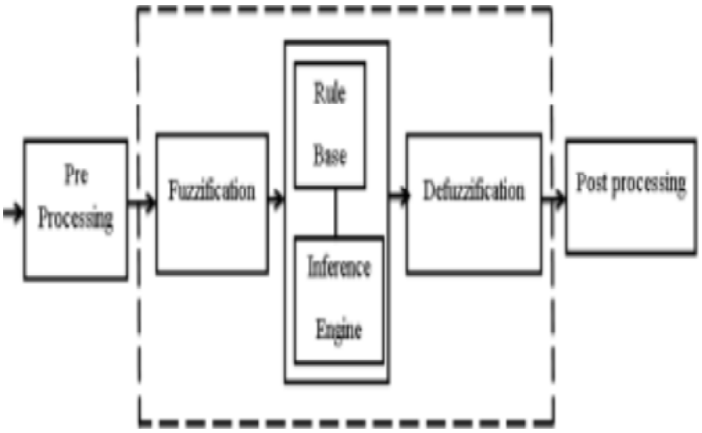

Figure 7: Fuzzy logic controller

Fuzzification: Membership function values are assigned to the linguistic variables, using seven fuzzy subsets: NB (Negative Big), NM (Negative Medium), NS (Negative Small), ZE (Zero), PS (Positive Small), PM (Positive Medium), and PB (Positive Big). The partition of fuzzy subsets and the shape of membership CE(k) E(k) function adapt the shape up to appropriate system. The value of input error and change in error are normalized by an input scaling factor.

Table 1
Fuzzy Rules

Change in Error	*NB*	*NM*	*NS*	*Z*	*PS*	*PM*	*PB*
NB	PB	PB	PB	PM	PM	PS	Z
NM	PB	PB	PM	PM	PS	Z	Z
NS	PB	PM	PS	PS	Z	NM	NB
Z	PB	PM	PS	Z	NS	NM	NB
PS	PM	PS	Z	NS	NM	NB	NB
PM	PS	Z	NS	NM	NM	NB	NB
PB	Z	NS	NM	NM	NB	NB	NB

In this system the input scaling factor has been designed such that input values are between -1 and +1. The triangular shape of the membership function of this arrangement presumes that for any particular E(k) input there is only one dominant fuzzy subset. The input error for the FLC is given as

$$E(k) = \frac{P_{ph(k)} - P_{ph(k-1)}}{V_{ph(k)} - V_{ph(k-1)}} \quad (22)$$

$$CE(k) = E(k) - E(k\text{-}1) \quad (23)$$

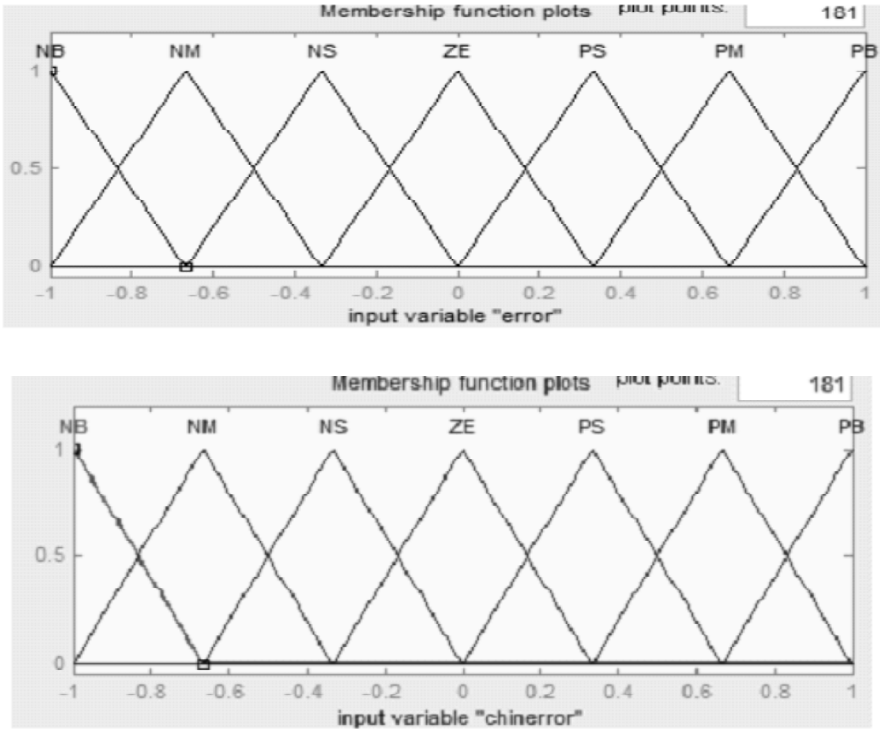

Figure 8: Membership functions

Inference Method: Several composition methods such as Max–Min and Max-Dot have been proposed in the literature. In this paper Min method is used. The output membership function of each rule is given by the minimum operator and maximum operator. Table 1 shows rule base of the FLC.

Defuzzificaion: As a plant usually requires a non-fuzzy value of control, a Defuzzificaion stage is needed. To compute the output of the FLC, „height method is used and the FLC output modifies the control output. Further, the output of FLC controls the switch in the inverter. In UPQC, the active power, reactive power, terminal voltage of the line and capacitor voltage are required to be maintained. In order to control these parameters, they are sensed and compared with the reference values. To achieve this, the membership functions of FC are: error, change in error and output.

The set of FC rules are derived from

$$u=-[\alpha E + (1-\alpha)*C] \quad (24)$$

VI. SIMULATION RESULTS

This section provides detailed information about the simulation and the system parameters used for the measurements. Furthermore, the acquired measurement results using the proposed concept are compared to a synchronous rectifier solution.

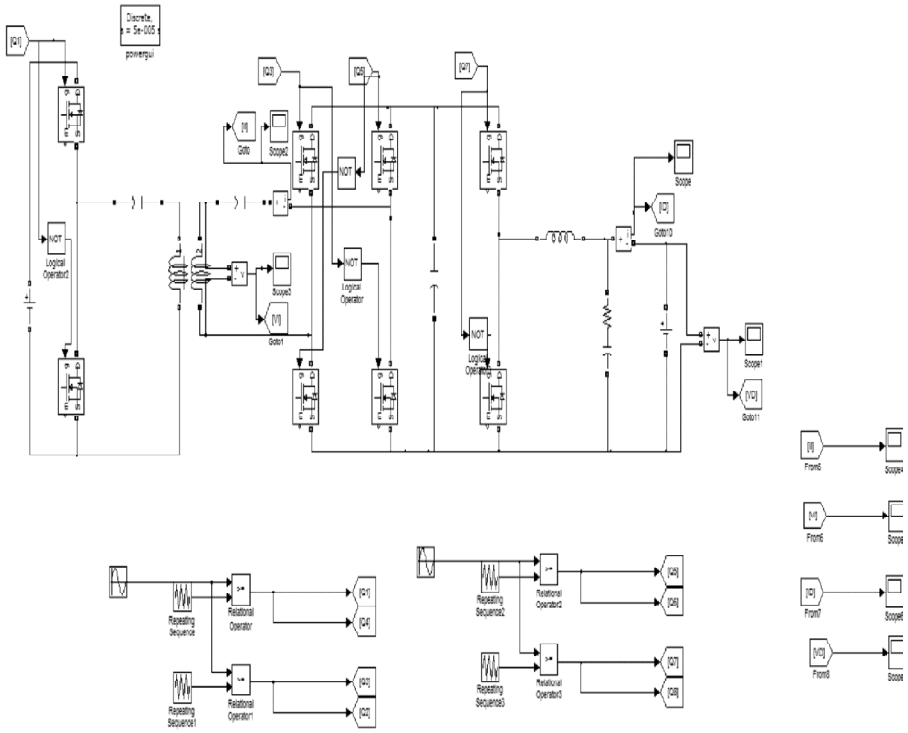

Figure 9: Simulation Design of the proposed method

In order to validate the proposed concept, the values of the phase-shift ϕ and the rectified voltage Vr, which is controlled by the duty cycleD of the dc–dc converter, have been adjusted during the measurements to achieve maximum efficiency for each value of the output power. For the synchronous rectification, a zero-crossing detection of the rectifier input current I_L is implementedand the full bridge (S_1– S_4) is driven accordingly.

The duty cycle D of the dc–dc converter is used to control the equivalent load resistance and hence the amount of power at the output of the system.When utilizing the proposed optimization method for a coupling factor k = 0.6, the measured point of maximum efficiency· = 77.3% is reached at an output power of Pout = 3 W with a phase-shift ϕ = 20° and a duty cycle D = 68%. Fig. 10(a) shows a measurement of the waveforms of the rectifier input voltage V_L and the input current I_L employing these conditions. Fig. 10(b) shows the same waveforms for the synchronous rectification approach using comparable conditions as in Fig. 10(a) (duty cycle D = 66%, output power Pout = 2.8 W and efficiency· = 75.9%).

As shown in Fig. 10, the proposed control method introduces a phase-shift between the input current I_L and the input voltageV_L of the active rectifier, while the synchronous rectification maintains a zero phase-shift behaviour of the system.

VII. CONCLUSION

This proposed method is to Maximize the efficiency as well on increase the amount of extractable power of a WPT system operating in no resonant operation a phase-shift control approach, instead of a conventional controlling technique, is applied to the active rectifier on the secondary aspect of an RPT system. This system is employed to attain efficiency improvements by modifying the secondaryside resonance frequency; however on the opposite hand it also impacts the equivalent load impedance. The theoretical background of the proposed concept has been presented and valid by simulations with the help of a WPT prototyping system based on the qi standard. The results show that the potency of the system will be exaggerated over the complete mensuration vary compared to a synchronous rectifier. Here we are using the fuzzy controller

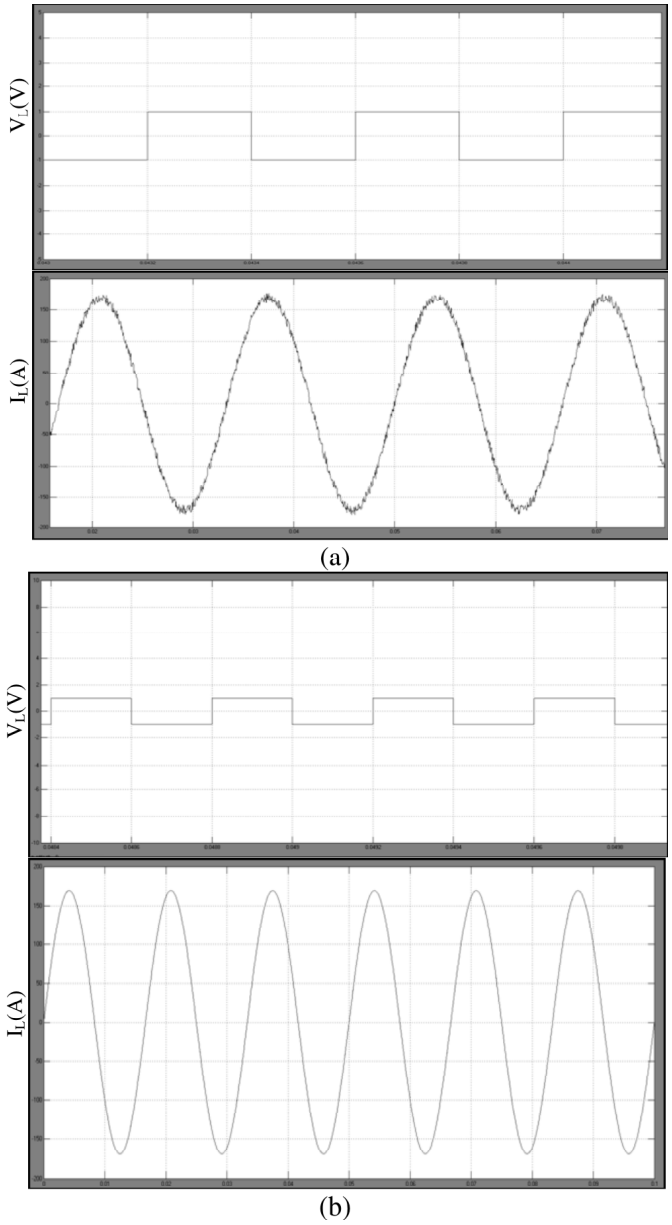

Figure 10: Measurement of the key system waveforms for the proposed concept and a synchronous rectification approach at k = 0.6. (a) Waveforms of the rectifier input voltage V_L (3V/div) and input current I_L (600 mA/div) for the proposed concept with a phase-shift of $\phi = 20°$ and a duty cycle D = 68%. (b) Waveforms of V_L (3V/div) and I_L (600 mA/div) for synchronous rectification with a duty cycle D = 66%

compared to other controllers Furthermore, the maximum extractable output power of the prototyping system is raised by 36% for a coupling factor k = 0.6, and even by 83% for a coupling factor of k = 0.3, again in comparison to a synchronous rectification approach.

REFERENCES

[1] A. RamRakhyani, S. Mirabbasi, and M. Chiao, "Design and optimization of resonance-based efficient wireless power delivery systems for biomedical implants," IEEE Trans. Biomed. Circuits Syst., vol. 5, no. 1, pp. 48–63, Feb. 2011.

[2] M. Zargham and P. Gulak, "Maximum achievable efficiency in near-field coupled power-transfer systems," IEEE Trans. Biomed. Circuits Syst., vol. 6, no. 3, pp. 228–245, Jun. 2012.

[3] R. Wu, W. Li, H. Luo, J. Sin, and C. Yue, "Design and characterization of wireless power links for brain machine interface applications," IEEE Trans. Power Electron., vol. 29, no. 10, pp. 5462–5471, Oct. 2014.

[4] G. Covic and J. Boys, "Modern trends in inductive power transfer for transportation applications," IEEE J. Emerg. Sel. Topics Power Electron., vol. 1, no. 1, pp. 28–41, Mar. 2013.

[5] S. Lukic and Z. Pantic, “Cutting the cord: Static and dynamic inductive wireless charging of electric vehicles,” IEEE Electrific. Mag., vol. 1, no. 1, pp. 57–64, Sep. 2013.

[6] S. Choi, J. Huh, W. Lee, and C. Rim, “Asymmetric coil sets for wireless stationary EV chargers with large lateral tolerance by dominant field analysis,” IEEE Trans. Power Electron., vol. 29, no. 12, pp. 6406–6420, Dec. 2014.

[7] S. Hui and W. Ho, “A new generation of universal contactless battery charging platform for portable consumer electronic equipment,” IEEE Trans. Power Electron., vol. 20, no. 3, pp. 620–627, May 2005.

[8] E. Waffenschmidt, “Wireless power for mobile devices,” in Proc. IEEE Int. Telecom. Energy Conf., 2011, pp. 1–9.

[9] A. Satyamoorthy, P. Riehl, H. Akram, Y.-C.Yen, J.-C.Yang, B. Juan, C.-M.Lee, and F.-C. Lin, “Wireless power receiver for mobile devices supporting inductive and resonant operating modes,” in Proc. IEEE Wireless Power Transfer Conf., 2014, pp. 52–55.

[10] S. Hui, W. Zhong, and C. Lee, “A critical review of recent progress in mid-range wireless power transfer,” IEEE Trans. Power Electron., vol. 29, no. 9, pp. 4500–4511, Sep. 2014.